

An optical differential reflectance study of adsorption and desorption of xenon and deuterium on Ni(111)

A. Wong, X.D. Zhu*

Department of Physics, University of California, Davis, CA 95616, USA
(Fax: + 1-916/752-4717, E-mail: xdzhu@ucdphy.ucdavis.edu)

Received: 6 November 1995/Accepted: 26 February 1996

Abstract. We studied adsorption and desorption of Xe and deuterium on Ni(111) using an optical differential reflectance technique. The main findings are: (i) the differential reflectance varies almost linearly with the surface densities of deuterium and Xe adatoms, and the signals can be described well with a three-layer model and the known dielectric responses of the surface layers; (ii) the adsorption of deuterium at $T = 120$ K follows the Langmuir kinetics, while the adsorption of Xe at $T = 38$ K follows the zeroth-order kinetics; (iii) near $T = 70$ K, the rate of Xe desorption is almost coverage-independent with an activation energy of $E_{\text{des}} = 4.4 \pm 0.2$ kcal/mol. Our analysis suggests that the Xe desorption is likely to be dominated by the escape rate from the corners of two-dimensional Xe islands.

PACS: 78.66; 82.65

As fundamental processes in gas–solid interactions, gas adsorption onto and desorption from a substrate are two of the most studied subjects in surface science [1]. An essential aspect in an experimental investigation of the gas adsorption is to ascertain the coverage of adsorbates. For this purpose, many techniques based upon electron emission properties or optical reflectance have been developed over the past decades. One of the most frequently used techniques is the work function method [1, 2]. This technique measures the work function change as a result of adsorption of atoms or molecules on metallic or semiconductor surfaces. The interaction of adsorbates with a surface, causes a charge rearrangement in the direction normal to the surface, which in turn alters the dipolar field across the surface. The latter changes the electron work function. After a calibration against, for example, mass yields during the thermal desorption, one can use the work function change as a secondary measure of the adsorbate coverage [3].

Optical reflectance techniques such as differential reflectance and optical surface second-harmonic generation are alternatives to the work function method [4–9]. Rather than sensing the change in the static dipole moment within the surface region, optical techniques measure the change in the dynamic dipole moment. They can be equally well calibrated by thermal desorption mass spectrometry [9]. The optical techniques have the advantage of being truly non-intrusive and remote-sensing methods. The linear optical techniques, when applicable, are usually more easily implemented than the nonlinear optical techniques. The change in the reflectivity of a metal surface due to a monolayer of adsorbates is very small, normally in the range of one part in 10^3 . Experimentally, one may eliminate the large background by measuring the differential reflectance of one type or another [4, 6, 7].

In this paper, we report a study of adsorption and isothermal desorption of Xe and deuterium on Ni(111) using a polarization *differential reflectance* technique. In our case, we measure the differential reflectance between *s*-polarized and *p*-polarized light. This technique has been demonstrated recently by Xiao et al. [6]. It is based upon the facts that the reflectance change for *s*- and *p*-polarized light as a result of gas adsorption are usually different. Like the work function method, such a difference can be exploited to measure the coverage of the adsorbates [6].

1 Experimental procedures

The experiment is conducted in an ultrahigh vacuum chamber with an operating pressure below 5×10^{-11} Torr. A Ni(111) sample disc is oriented with a miscut angle less than 0.1° . The surface of the sample is cleaned with short cycles of Ne^+ ion sputtering and annealing at 1100 K. Cleanliness is examined with an Omicron LEED-Auger system and less than 0.2% of a monolayer (the limits of the detection system) of sulfur and carbon were detected. The cleaned Ni(111) exhibits a sharp (1×1) LEED pattern. Through a combination of electron beam heating and cryogenic cooling with a close-cycle helium

*To whom all correspondence should be addressed.

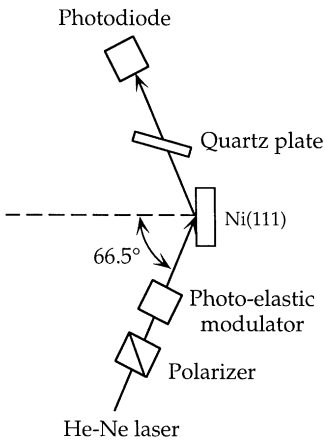


Fig. 1. Optical differential reflectance setup. The He–Ne laser is initially *s*-polarized

refrigeration system (CRYOMECH GB220), we can vary the sample temperature from 28 to 1500 K. The temperature is monitored with a chromel–alumel thermocouple spot-welded to the side of the Ni sample disc. The reference junction of the thermocouple is immersed in liquid nitrogen.

For adsorbates, we use the deuterium gas of 99.7% purity from Liquid Carbonic and Xe gas of 99.995% purity from Airco. The purity of gases is further verified with a UTI 100C quadrupole mass spectrometer on the ultrahigh vacuum chamber. During adsorption measurements, we backfill the chamber with the gas of interest. The partial pressure is measured with a Varian Bayard–Albert ion gauge and is corrected against the appropriate ionization calibration factors for Xe and deuterium.

The sketch of our optical setup is shown in Fig. 1. We use a 2 mW polarized He–Ne laser as the probe. The incidence angle is set at $\Phi_{\text{inc}} = 66.5^\circ$. For the differential reflectance measurements, we employ a photo-elastic modulator (Hinds Instruments PEM90) in the optical path to alter the polarization of the laser beam from *s*- to *p*-polarization at a frequency of $\Omega = 50$ kHz. Also inserted in the beam path is a tilted fused quartz parallel plate. It is used to introduce an imbalance in transmittance between *s*- and *p*-polarization to offset the difference in reflectance between the two polarizations from the bare Ni(111) surface. We detect the reflected light with a lock-in amplifier at the second harmonics of the modulation frequency. This component is proportional to the differential reflectance between *s*- and *p*-polarization [6, 10],

$$I_{\text{out}}(2\Omega) = c' [|r_s(\Phi_{\text{inc}})t_s(\Phi_{\text{tilt}})|^2 - |r_p(\Phi_{\text{inc}})t_p(\Phi_{\text{tilt}})|^2] I_0, \quad (1)$$

$r_s(\Phi_{\text{inc}})$ and $r_p(\Phi_{\text{inc}})$ are the reflectivities of the sample Φ_{tilt} is the tilt angle of the quartz plate. $t_s(\Phi_{\text{tilt}})$ and $t_p(\Phi_{\text{tilt}})$ are the transmission coefficients of the quartz plate. $c' = J_2(\pi) = 0.485$ [10]. I_0 is the intensity of the incident He–Ne laser. In a typical measurement, we first minimize the differential reflectance signal by adjusting the tilt angle

Φ_{tilt} of the fused quartz plate such that

$$|r_s^{(0)}(\Phi_{\text{inc}})t_s(\Phi_{\text{tilt}})|^2 = |r_p^{(0)}(\Phi_{\text{inc}})t_p(\Phi_{\text{tilt}})|^2.$$

$r_s^{(0)}(\Phi_{\text{inc}})$ and $r_p^{(0)}(\Phi_{\text{inc}})$ denote the reflectivities of the bare Ni(111) surface. Subsequently, we backfill the chamber with the gas of interest and monitor the change in the differential reflectance. D_2 and Xe *do not* adsorb on the optical windows at room temperature. Adsorption of Xe or deuterium changes the reflectivities to

$$r_s(\Phi_{\text{inc}}) = r_s^{(0)}(\Phi_{\text{inc}})[1 + i\Delta_s(\Phi_{\text{inc}})] \quad \text{and}$$

$$r_p(\Phi_{\text{inc}}) = r_p^{(0)}(\Phi_{\text{inc}})[1 + i\Delta_p(\Phi_{\text{inc}})],$$

respectively [4]. The change in differential reflectance can be written as

$$I_{\text{out}}(2\Omega) = 0.485 I_R [\text{Im}\{\Delta_p(\Phi_{\text{inc}})\} - \text{Im}\{\Delta_s(\Phi_{\text{inc}})\}], \quad (2)$$

$I_R \equiv I_0 |r_s^{(0)}(\Phi_{\text{inc}})t_s(\Phi_{\text{tilt}})|^2$ is the intensity of the reflected He–Ne beam without modulation. $\Delta_s(\Phi_{\text{inc}})$ and $\Delta_p(\Phi_{\text{inc}})$ are functions of the adsorbate coverage θ through the dielectric constant of the surface layer. As shown in the next section, we found that the differential reflectance changes almost linearly with the coverage for both deuterium (up to $\theta = 0.7$) and Xe (up to $\theta = 0.33$) on Ni(111).

2 Results and discussion

2.1 Adsorption of deuterium on Ni(111)

It is fairly well established in the literature and reproducible in our measurement that deuterium molecules adsorb onto Ni(111) dissociatively at temperatures up to and slightly above 300 K [3, 11]. At coverages below 50% of a monolayer (i.e., $\theta \leq 0.5$), deuterium atoms occupy equally the fcc and hcp three-fold hollow sites. In the Thermal Desorption mass Spectrometry (TDS), these adsorbed deuterium atoms form the so-called β_2 peak with an associative desorption energy of 23 kcal/mol [3]. At $\theta = 0.5$, deuterium adatoms form a $C(2 \times 2)$ overlayer structure. At coverages above 50% of a monolayer up to one monolayer, Christmann and co-workers suggested, based upon their LEED and thermal desorption analysis, that the excessive deuterium also adsorb dissociatively and may reside at on-top sites [11]. These excessive deuterium adatoms are identified in the thermal desorption as the β_1 peak. So far, the exact adsorption sites of these β_1 deuterium adatoms remain to be fully resolved.

In Fig. 2, we display the differential reflectance from Ni(111) [curve (a)] vs the deuterium dosage [in unit of Langmuir (L), 1 Langmuir = 10^{-6} Torr-s]. The sample temperature is kept at $T = 120$ K. The dosing pressure of deuterium is at 2.6×10^{-8} Torr. The signal levels off after about 10 L. The initial cancellation in the present experiment is roughly $1 \times 10^{-5} I_R$ and is limited by the precision of the angular adjustment of the quartz plate and the mechanical instability of the optical setup. To calibrate the differential reflectance against the coverage, we performed a series of adsorption measurements with different dosages. Each optical measurement is followed by a

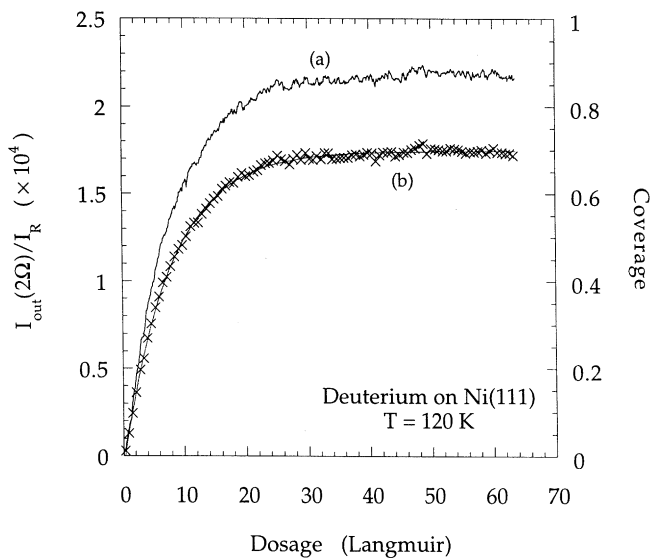


Fig. 2. **a** Normalized differential reflectance from Ni(111) vs deuterium dosage at $T = 120$ K (see (2) for the definitions of $I_{\text{out}}(2\Omega)$ and I_{R}). **b** Dissociative adsorption isotherm of deuterium on Ni(111) at $T = 120$ K, deduced from **a** and Fig. 3. The solid line is a fit to Langmuir kinetics model $\theta(D) = \theta_s \exp(-S_0 \Gamma D / N_s \theta_s p)$

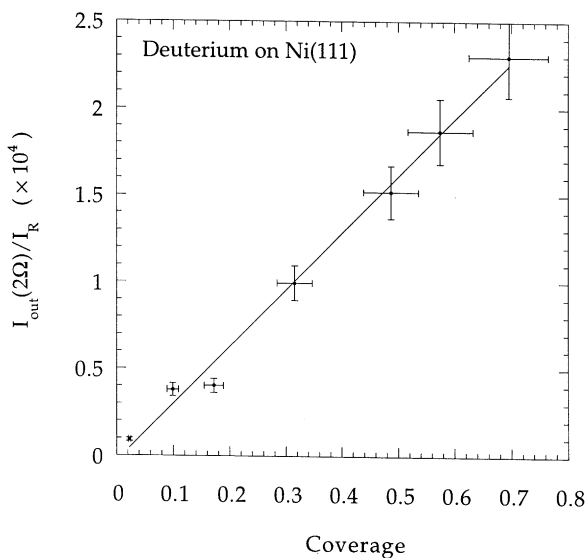


Fig. 3. Normalized differential reflectance vs the deuterium coverage deduced from the thermal desorption mass yields. The solid line is a fit to a linear function

thermal desorption mass yield measurement. We use the time-integrated pressure under the maximum β_2 peak as the measure of $\theta = 0.5$. This procedure yields a 10% relative error in the coverage determination (limited by the thermal desorption mass yield measurements). In Fig. 3, we show the result of such an empirical calibration. The optical signal varies linearly with the coverage up to $\theta = 0.7$. The calibrated differential reflectance is later used to determine the deuterium coverage with an absolute precision of less than 2% (limited by the optical measurements) and a relative error of 10%. We note that the

differential reflectance change at $\theta = 0.7$ is $I_{\text{max}}^{\text{deuterium}}(2\Omega) = 2.3 \times 10^{-4} I_{\text{R}}$. The origins of the differential reflectance from deuterium-covered Ni(111) can be understood fairly well within the standard three-layer model, consisting of the vacuum region, a surface layer, and the nickel bulk region [4, 5]. The surface layer is defined as the region between the vacuum and the nickel substrate with an optical response different from those of the two adjoining bulk media. The linear dielectric constant of the surface layer $\epsilon_s = 1 + 4\pi\chi_s$ is a function of the coverage of adsorbates. For deuterium on Ni(111) which is a typical case of strong chemisorption, we expect the surface layer to be the topmost atomic layer of the Ni substrate. Upon adsorption of deuterium, the layer transforms into a deuterated nickel hydride. The optical dielectric constant of a nickel hydride on top of Ni(111) is not available directly. We estimate the nickel hydride optical constant from the photoemission and the inverse photoemission studies of hydrogen adsorption on Ni(111) [12–14]. The energy states of interest are those within 2.0 eV above and below Ni Fermi surface since the single photon energy of a He–Ne laser is 1.96 eV. The most relevant experimental work is that by Frank and co-workers [12]. They measured both the normal photoemission and the inverse photon emission of a monolayer epitaxially grown Ni(111) on Cu(111) with and without adsorbed hydrogen. The lattice constant of the epitaxial Ni layer is only 2.5% larger than that of the bulk Ni and thus we do not expect it to have a significant effect on the electron energy state distribution near the Fermi surface [15]. Such an epitaxial layer is a good approximation to the surface layer in our case. The results of these authors show that the most prominent changes in the joint density of states occur for transitions from 1.8 eV below the Fermi level to 0.2 eV above the Fermi level and from just below the Fermi level to 2.0 eV above the Fermi level. The total joint density of states (including both transitions) for a hydrogen-covered epitaxial Ni(111) layer decreases by 22% from that of a clean epitaxial Ni(111) layer. If we assume that the optical dielectric constant is simply proportional to the joint density of states of these relevant transitions, we arrive at an estimate of the dielectric constant of a nickel hydride on Ni(111) $\epsilon_{\text{Ni-H}} = 0.78\epsilon_{\text{Ni}}$. The optical response of a deuterated nickel hydride is expected to be essentially the same as a nickel hydride. Using the results of Aspnes and McIntyre [4], the differential reflectance change at the deuterium coverage $\theta = 0.7$ is given by (2) with

$$\Delta_p(\Phi_{\text{inc}}) = - \left(\frac{4\pi d_{\text{Ni-H}} \cos \Phi_{\text{inc}}}{\lambda} \right) \times \frac{\epsilon_{\text{Ni}}^2 (\epsilon_{\text{Ni-H}} - \sin^2 \Phi_{\text{inc}}) - \epsilon_{\text{Ni-H}}^2 (\epsilon_{\text{Ni}} - \sin^2 \Phi_{\text{inc}})}{\epsilon_{\text{Ni}} \epsilon_{\text{Ni-H}} \cos^2 \Phi_{\text{inc}} - \epsilon_{\text{Ni-H}} (\epsilon_{\text{Ni}} - \sin^2 \Phi_{\text{inc}})} \quad (3)$$

$$\Delta_s(\Phi_{\text{inc}}) = - \left(\frac{4\pi d_{\text{Ni-H}} \cos \Phi_{\text{inc}}}{\lambda} \right) \frac{\epsilon_{\text{Ni}} - \epsilon_{\text{Ni-H}}}{\epsilon_{\text{Ni}} - 1}. \quad (4)$$

Using the dielectric constant of bulk Ni $\epsilon_{\text{Ni}} = -10.06 + i14.77$ and $d_{\text{Ni-H}} = 2.49 \text{ \AA}$, we obtain a calculated differential reflectance of $I_{\text{out}}(2\Omega) = 3.6 \times 10^{-4} I_{\text{R}}$. This value compares favorably with the experimental value of

$I_{\max}^{\text{deuterium}}(2\Omega) = 2.3 \times 10^{-4} I_R$. We have also calculated the coverage dependence of the differential reflectance and the latter is very close to a linear function as what we have observed.

From the calibration and curve (a) in Fig. 2, we obtain an adsorption isotherm $\theta(D)$ at $T = 120$ K shown as curve (b) in Fig. 2. D is the dosage in units of Langmuir. The result fits very well to a Langmuir kinetics model which assumes the sticking probability to be proportional to the number of unoccupied sites and thereby $\theta(D) = \theta_s \exp(-2S_0\Gamma D/N_s\theta_s p)$ [16]. The factor 2 in the exponent arises from the fact that each D_2 molecule dissociates into two atoms and thus takes up two sites. From the fit we find $2S_0\Gamma/N_s\theta_s p = 0.12 \text{ L}^{-1}$. Since $\theta_s = 0.7$, $\Gamma/p = 1.0 \times 10^{15} \text{ cm}^{-2} \text{ L}^{-1}$ for D_2 at $T = 300$ K, and $N_s = 1.53 \times 10^{15} \text{ cm}^{-2}$ for Ni(111), we find the initial sticking coefficient $S_0 = 0.064$. This result agrees with the observation of Lapujoulade and Neil [17].

2.2 Adsorption and desorption of Xe

2.2.1 Adsorption of Xe on Ni(111). The physisorption of Xe on Ni(111) is conducted at temperatures below 73 K. At $T = 68.5$ K, the differential reflectance changes slightly and levels off to $3 \times 10^{-5} I_R$ at Xe partial pressures up to 2×10^{-8} Torr. Upon raising the Xe pressure to 3.4×10^{-8} Torr, the signal increases dramatically and levels off at $I_{\max}^{\text{Xe}} = 4.5 \times 10^{-4} I_R$. The differential reflectance signal remains unchanged even when we raise the Xe pressure to 7×10^{-7} Torr (by a factor of 20). This plateau feature is found ubiquitous for inert gas adsorption on metals and it is indicative of the formation of the first layer of Xe atoms on Ni(111) [18–32]. Xe adatoms desorb as soon as the pressure is reduced. Thus the first Xe overlayer is maintained dynamically in the pressure range from 3.4×10^{-8} Torr to 7×10^{-7} Torr. The sharp pressure dependence of the coverage suggests that the desorption of Xe is most likely to be *coverage-independent* (i.e., of zeroth order) [18–20]. The latter is confirmed in the subsequent isothermal desorption measurements which we will present shortly. To calibrate the differential reflectance against the Xe coverage, we conducted a series of adsorption measurements at $T = 38$ K where the desorption rate of Xe adatoms from the first overlayer is negligible compared to the adsorption rate. In Fig. 4, we show the differential reflectance [curve (a)] vs the Xe dosage. By performing the thermal desorption mass yield measurement following each optical measurement, we obtain a calibration of the differential reflectance vs the coverage as shown in Fig. 5. The saturation coverage $\theta_s = 0.33$ is deduced from the observation of a sharp $(\sqrt{3} \times \sqrt{3})R30^\circ$ overlayer structure. The latter is shown in Fig. 6a, b. The optical signal varies almost linearly with the Xe coverage except for a small and yet noticeable curvature at coverages above 0.2. The result is a best fit to a polynomial of second degree. Using the calibration, we obtain the adsorption isotherm of Xe at $T = 38$ K which is also displayed in Fig. 5 as curve (b). Unlike deuterium on Ni(111), the Xe coverage increases linearly with the dosage almost up to the saturation coverage. This means that the stick-

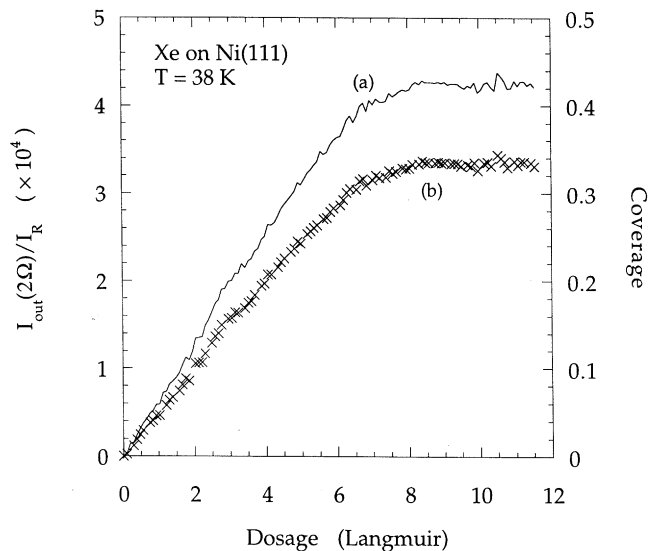


Fig. 4. Normalized differential reflectance from Ni(111) vs the Xe dosage at $T = 38$ K **b** Adsorption isotherm of Xe on Ni(111) at $T = 38$ K, deduced from (a) and Fig. 5

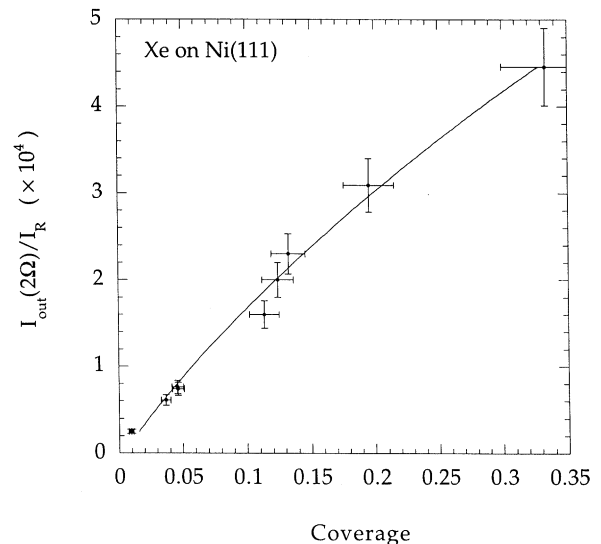


Fig. 5. Normalized differential reflectance vs Xe coverage deduced from the thermal desorption mass yields. The solid line is a fit to a polynomial of second degree

ing probability for Xe is independent of the probability of finding unoccupied sites [18–20]. From the slope of the isotherm $S_0\Gamma/N_s p = 0.043 \text{ L}^{-1}$ and the facts that $\Gamma/p = 1.8 \times 10^{14} \text{ cm}^{-2} \text{ L}^{-1}$, we deduce the sticking probability $S_0 = 0.35$. Such a high sticking probability is also observed consistently on many other metal surfaces including graphite (0001) [18–20, 27].

We note that the overlayer structure at $\theta_s = 0.33$ appears commensurate with the underlying Ni(111) lattice. This is consistent with the fact that the Xe–Xe separation $d_{\text{Xe-Xe}}$ on Ni(111) at $\theta_s = 0.33$ is 4.31 \AA which is compressed from the bulk equilibrium value of 4.34 \AA by only 0.7%. Such a small compression costs only a 0.15%

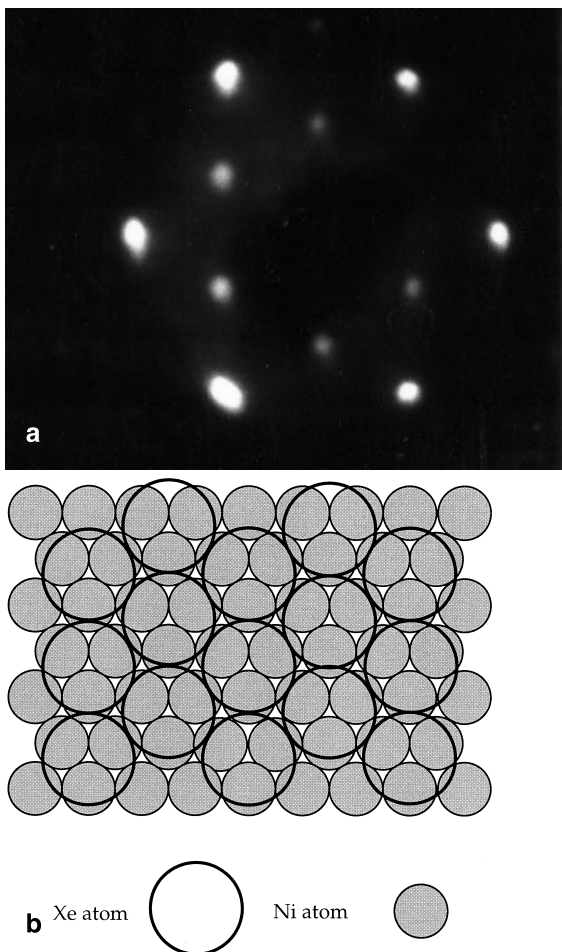


Fig. 6. a Low-Energy-Electron Diffraction (LEED) pattern of the Xe overlayer on Ni(111) at the saturation coverage of $\theta_s = 0.33$ at $T = 38$ K. The electron energy is 194 eV. The outer six diffraction spots arise from the Ni(111) substrate. The inner six spots (one blocked by the electrical leads) arise from the Xe overlayer structure. The real-space overlayer structure is a commensurate $(\sqrt{3} \times \sqrt{3})R30^\circ$ overlayer structure as illustrated in **b. b** Real-space $(\sqrt{3} \times \sqrt{3})R30^\circ$ overlayer structure of Xe on Ni(111) at the saturation coverage of $\theta_s = 0.33$

change in the Xe–Xe pair interaction energy and should not disfavor the commensurate $(\sqrt{3} \times \sqrt{3})R30^\circ$ overlayer structure. Xe also forms the commensurate $(\sqrt{3} \times \sqrt{3})R30^\circ$ structure on the (111) faces of a number of other fcc transition metals such as Cu (with $d_{\text{Xe-Xe}} = 4.42$ Å), Pd (with $d_{\text{Xe-Xe}} = 4.76$ Å) and even Pt (with $d_{\text{Xe-Xe}} = 4.80$ Å). On Ni(100) on the other hand, Xe adatoms are found to form incommensurate structures. This is understandable as the two nearest neighbor distances between four-fold hollow sites on Ni(100) are 3.52 Å and 4.98 Å. At the separation of 3.52 Å, the Xe–Xe interaction is strongly repulsive and therefore extremely unstable. At the separation of 4.98 Å, the Xe–Xe interaction, though still attractive, is reduced in strength by 32% from its bulk value. Consequently, the commensurate overlayer structure is often subject to the competition of incommensurate structures. Similar arguments apply to Pt(100), Cu(100) and Pd(100).

Xe on Ni(111) is a typical case of physisorption. In this case, the surface layer can be reasonably assumed to consist of a layer on top of Ni(111) with a thickness of the Xe diameter. The dielectric constant of the layer changes from that of the vacuum to that of the bulk Xe. The Ni(111) substrate remains unchanged. We find that such a simple model yields a rather satisfactory signal strength when compared with the experimental observation. Again using the results of McIntyre and Aspnes [4], the differential reflectance change at the saturation coverage $\theta_s = 0.33$ is given by (2) with

$$A_p(\Phi_{\text{inc}}) = - \left(\frac{4\pi d_{\text{Xe}} \cos \Phi_{\text{inc}}}{\lambda} \right) \times \frac{\epsilon_{\text{Ni}}^2 (\epsilon_{\text{Xe}} - \sin^2 \Phi_{\text{inc}}) - \epsilon_{\text{Xe}}^2 (\epsilon_{\text{Ni}} - \sin^2 \Phi_{\text{inc}})}{\epsilon_{\text{Ni}}^2 \epsilon_{\text{Xe}} \cos^2 \Phi_{\text{inc}} - \epsilon_{\text{Xe}} (\epsilon_{\text{Ni}} - \sin^2 \Phi_{\text{inc}})}, \quad (5)$$

$$A_s(\Phi_{\text{inc}}) = - \left(\frac{4\pi d_{\text{Xe}} \cos \Phi_{\text{inc}}}{\lambda} \right) \frac{\epsilon_{\text{Ni}} - \epsilon_{\text{Xe}}}{\epsilon_{\text{Ni}} - 1}. \quad (6)$$

Using the dielectric constant of bulk Xe $\epsilon_{\text{Xe}} = 1.4$ and $d_{\text{Xe}} = 4.35$ Å, we arrive from the three layer model at a differential reflectance of $I_{\text{out}}(2\Omega) = 7 \times 10^{-4} I_R$. This value compares very favorably with the experimental value of $I_{\text{max}}^{\text{Xe}} = 4.5 \times 10^{-4} I_R$. Furthermore, the calculated coverage dependence of the differential reflectance has a small curvature which essentially reproduces what we observed experimentally (Fig. 5).

2.2.2 Desorption of Xe from Ni(111). Desorption kinetics of a noble gas on many metals have been studied extensively [18–32]. This is in part motivated by the relatively simple forms of interactions among adsorbed noble gas atoms and the underlying substrates. Desorption activation energies for Xe from metal surfaces vary from 4 to 11 kcal/mol. The variation with different index planes of a number of metals such as W and Pd is consistent with a simple coordination model [29, 31]. The model assumes that the binding energy of desorption is proportional to a sum of pair-wise Lennard–Jones interaction energy between a Xe adatom and its nearest neighbor substrate atoms. From metal to metal, the activation energies do vary substantially even on the same Miller index plane [e.g., 9.4 kcal/mol for Xe on Pd (100) and 5.2 kcal/mol for Xe on Ni(100)]. Both zeroth order (the rate being independent of the coverage) and first-order (the rate being linearly proportional to the coverage) desorption kinetics have been reported for Xe. For example, zeroth order desorption were observed on Cu(100), W(110) and graphite (0001) [18–20, 32]. On other metals including Ni(100), the desorption of Xe was found to be of first-order. Our calibrated differential reflectance probe is conveniently suited for the investigation of adsorbate desorption kinetics [22, 30–32].

We studied the isothermal desorption of Xe at a series of temperatures near 70 K. At each temperature, we first expose the Ni(111) surface to Xe at a pressure 7×10^{-7} Torr until the differential reflectance levels off at the saturation coverage $\theta_s = 0.33$. We then evacuate the vacuum chamber at a rate such that the pressure drops from 7×10^{-7} Torr to below 3×10^{-10} Torr in 3–4 s. The

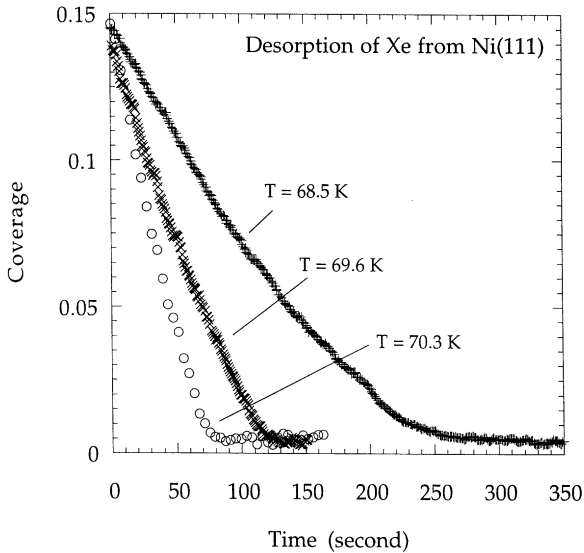


Fig. 7. The time evolution of Xe coverage during the isothermal desorption from Ni(111) at temperatures near 70 K

evolution of the differential reflectance is recorded immediately after the Xe partial pressure dips below 3×10^{-10} Torr. Using the calibration between the differential reflectance and the Xe coverage, we obtain the evolution of the coverage during the isothermal desorption. The results are displayed in Fig. 7. The coverage decreases essentially linearly with time. This means that the rate of desorption is *independent of the Xe coverage* and therefore the desorption is zeroth order [18–20, 32]. The zeroth order desorption behavior is also consistent with the presence of a critical pressure p_c during the Xe adsorption at $T = 68.5$ K ($p_c = 3.4 \times 10^{-8}$ Torr). In this case, when the pressure is below p_c , the coverage-independent desorption rate from the first layer is always larger than the adsorption rate (assuming a coverage-independent sticking probability) and thus the Xe coverage remains close to zero. When the pressure is above p_c , the adsorption rate is always larger than the desorption rate and the Xe coverage continues to increase until the first layer of Xe is completed. This is indeed what we observed. The zeroth order desorption is described by the equation,

$$\frac{d\theta}{dt} = -v_0 \exp\left(-\frac{E_{\text{des}}}{RT}\right) \quad (7)$$

and the rate is given by $v_0 \exp(-E_{\text{des}}/RT)$. In Fig. 8, we show the Arrhenius plot of the desorption rates. From a fit to an Arrhenius function, we extract the Xe desorption activation energy of $E_{\text{des}} = 4.4 \pm 0.2$ kcal/mol and the pre-exponential factor $v_0 = 3.4 \times 10^{11} \text{ s}^{-1}$. The activation energy extracted from our measurements differs from the isosteric heat of adsorption $E_{\text{des}} = 7.3$ kcal/mol reported by Dolle and co-workers [33]. This is somewhat surprising. Since the isosteric heat measurements were performed at *higher* temperatures, one would expect more Xe atoms to be in an adsorbed gas phase with *smaller* binding energies. Because the Ni(111) sample used in the study of Dolle et al. has a much larger miscut angle (around 1°), it might be possible that at higher temper-

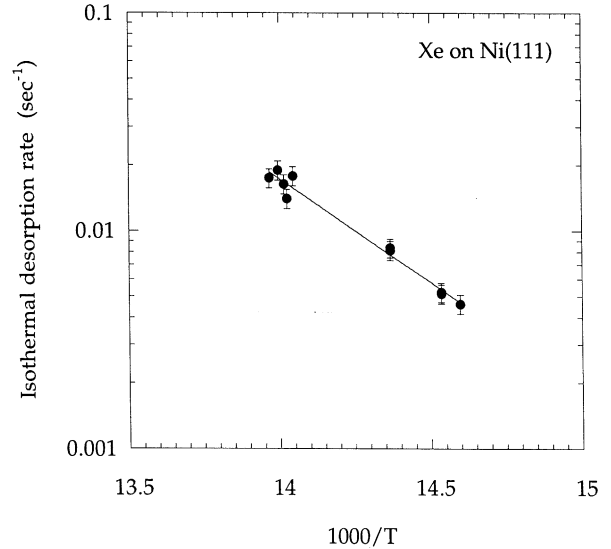


Fig. 8. Arrhenius plot of the isothermal desorption rate vs the nickel substrate temperatures. The solid line is a fit to an Arrhenius function $v_0 \exp(-E_{\text{des}}/RT)$ which yields an activation energy of $E_{\text{des}} = 4.4 \pm 0.2$ kcal/mol and a pre-exponential factor $v_0 = 3.4 \times 10^{11} \text{ s}^{-1}$

atures the Xe desorption in their study occur preferentially from steps with a larger activation energy and larger pre-exponential factor. It is noteworthy that isosteric heats for Xe on similar fcc metals such as Pd increase with more open surfaces, following an ordering of $E_{\text{des}}(111) < E_{\text{des}}(100) < E_{\text{des}}(110)$ [29]. Our result on Ni(111) ($E_{\text{des}} = 4.4 \pm 0.2$ kcal/mol) and the result of Christmann and Demuth on Ni(100) ($E_{\text{des}} = 5.2$ kcal/mol) follow the same trend.

Since the separation between Xe on Ni(111) at the saturation coverage $\theta = 0.33$ (4.31 \AA) is very close to the diameter of Xe atom in its bulk solid phase (4.34 \AA), it is conceivable that the Xe adatoms form more stable islands on Ni(111) than on Ni(100) and consequently the desorption from Ni(111) may be strongly affected by the Xe–Xe interaction involved stable islands. Next we explore possible desorption models involving relatively stable Xe islands that may lead to a zeroth order desorption kinetics.

Zeroth order desorption of Xe are also observed on a number of other substrates such as graphite (0001), Cu(100) and W(110) [18–20, 32]. Venables and Bienfait suggested a model that they claim might result in a zeroth order desorption. In this model, they assumed that (1) a solid phase and two adsorbed gas phases (two-dimensional gases) coexist on graphite (0001). One adsorbed gas phase (G1) resides directly on the substrate, the other (G2) resides on top of the solid phase; (2) the desorption occurs only from the two adsorbed gas phases; (3) the desorption rate from the solid phase covered portion of the surface A is *only* proportional to the difference between the evaporation rate R_2 of G2 and the impinging rate R and the area A , the desorption rate from the rest of the surface $(1 - A)$ is *only* proportional to the difference of the evaporation rate R_1 of G1 and the impinging rate R and the area $1 - A$. The overall desorption rate from the surface is then given by $d\theta/dt = (R - R_1)(1 - A) + (R - R_2)A$. At

the equilibrium vapor pressure, the two evaporation rates must be equal so that the overall desorption rate becomes independent of the fractional area A . They then asserted that the desorption process is of zeroth order by setting the impinging rate R to zero. As pointed out by Opila and Gomer, this model implicitly assumes that the sticking coefficients onto the bare substrate and the solid-phase Xe are equal [32]. In the case of Xe on Ni(111), it is an open question whether this assumption would hold when the Xe gas temperature is reduced to 70 K. At the gas temperature of 300 K, our measurement yields a sticking probability of $S_0 = 0.35$, which is far from unity.

Opila and Gomer have explored two other models involving significant contributions from Xe islands [32]. The first model assumes that the desorption occurs from the perimeter of Xe islands directly into the vapor phase. The rate is then proportional to the product of the number of islands and the average circumference, $d(N_s \theta)/dt = -2\pi r N k_1 = -(2\theta/r) k_1$. r is the average radius of islands and $N = \theta/\pi r^2$ is the total number of islands per unit area. k_1 is the detachment rate per unit length from the perimeter of islands into the vapor phase. The shapes of Xe islands are assumed to be circular. By expressing $k_1 = (v_1/d_{Xe}) \exp(-E/RT)$, the desorption equation is rewritten as $d\theta/dt = -(2\theta/N_s d_{Xe} r) v_1 \exp(-E/RT)$ with the rate being $(2\theta/N_s d_{Xe} r) v_1 \exp(-E/RT)$. N_s is again the surface density of the substrate atoms. The rate becomes *coverage independent* or of zeroth order if θ/r remains constant or equivalently the number of islands per unit area $N = \theta/\pi r^2$ varies as $1/\sqrt{\theta}$. Using our experimental results and an initial island size of 20–60 Å, we obtain a detachment pre-exponential factor $v_1 \approx 9.3 \times 10^{12} \text{ s}^{-1}$ to $3.1 \times 10^{13} \text{ s}^{-1}$ and the detachment energy of $E_{des} = 4.4 \pm 0.2 \text{ kcal/mol}$. These numbers are reasonable. However, one obvious difficulty with this model is to justify physically why the number of islands should change with the coverage as $1/\sqrt{\theta}$. The second model of Opila and Gomer assumes that when Xe atoms detach from the edges of solid-phase islands, they move as two-dimensional gas with a thermal velocity $\bar{v} = \sqrt{k_B T/2m_{Xe}}$ until they strike other islands and get reattached. The desorption occurs when Xe is in the two-dimensional dilute gas phase. If the density of the latter is much smaller than that of the Xe islands, Opila and Gomer showed that, the desorption is *nearly coverage independent* as long as the island diameter is much larger than the size of a single Xe atom. The problem with the model is that even at temperatures above 70 K, isolated Xe atoms on transition metals have been shown to behave much like a lattice gas rather than a two-dimensional gas such that they move along the surface by incoherent hopping from one stable site to a neighboring site [34]. Consequently, the desorption rate should be inversely proportional to the size of the Xe islands and thereby vary as $1/\sqrt{\theta}$ rather than independent of the coverage.

We here suggest another model that requires more easily justified assumptions. From our experimental results, we observe that the zeroth order behavior remains down to very low coverage. This indicates that if there are islands, they tend not to break up on Ni(111) even down to fairly low coverages at around 70 K. It is then reasonable to consider tightly bound islands that have energeti-

cally favorable geometry such as triangles and hexagons. If we assume that the desorption occurs preferentially from the corners of Xe islands which have the fewest nearest-neighbors and thereby the smallest binding energy and that the total number of islands and their geometric shapes remain essentially unchanged, the desorption will exhibit a zeroth order behavior. Within our model, the desorption rate remains coverage independent until the island sizes drop to 3 atoms (triangular) or 7 atoms (hexagonal) in size, corresponding to coverages less than $\theta = 0.01$. This is consistent with the experimental observation. One possible justification for having a constant number of islands can be that the islands are stabilized by the relatively small number of defect sites on Ni(111) surface. In this case, the desorption rate is written as $d\theta/dt = -(N_c \theta/N_s \pi r^2) v_1 \exp(-E/RT)$ where N_c is the average number of corners on an island and $v_1 \exp(-E/RT)$ is the detachment rate from the island corner directly into the vapor phase. If the island number density is that of the defect density which is roughly $\theta/\pi r^2 = 0.002 N_s$, the initial island size will be 30 Å containing roughly 50 Xe atoms. Using $N_c = 6$ and our experimental results, we obtain the pre-exponential factor for the corner desorption $v_1 = 3.1 \times 10^{13} \text{ s}^{-1}$ and the corresponding activation energy $E_{des} = 4.4 \pm 0.2 \text{ kcal/mol}$. These numbers again are quite reasonable. We note that at the equilibrium separation of 4.31 Å, the Xe–Xe interaction energy for a corner atom varies between 0.62 kcal/mol (two neighbors) to 0.93 kcal/mol (three neighbors). From the desorption activation energy $E_{des} = 4.4 \pm 0.2 \text{ kcal/mol}$, this suggests that the Xe–Ni interaction energy is 3.5–3.8 kcal/mol at a three-fold hollow site. If this estimate is correct, we expect the Xe–Ni binding energy to increase by 33% on Ni(100) to 4.7–5.1 kcal/mol as Xe is expected to adsorb on a four-fold hollow site [30]. This value compares favorably with the desorption energy of 5.2 kcal/mol on Ni(100) reported by Christmann and Demuth. In a scanning tunneling microscopy measurement of Xe on Pt(111) (a similar fcc transition metal surface) at $T = 4 \text{ K}$, Weiss and Eigler found that Xe adatoms indeed form compact islands such as elongated hexagons [35]. Once a corner atom desorbs, the remaining atoms are expected to rapidly rearrange themselves to form a near-hexagon to minimize the total energy [36].

3 Conclusion

We have investigated the adsorption and desorption of Xe and deuterium on Ni(111) using a polarization-differential reflectance technique. We find that the absolute magnitude and the coverage dependence of the differential reflectance signals are described well with the standard three-layer model and the experimentally determined optical responses of the surface layers in both deuterium/Ni(111) and Xe/Ni(111). We find that the adsorption of deuterium follows the Langmuir kinetics. For Xe, we find that both the adsorption and desorption follow zeroth order kinetics, namely, are *coverage-independent*. Our analysis suggests that the observed zeroth order desorp-

tion kinetics is most likely to be dominated by the desorption from the corners of Xe islands.

Acknowledgements. This work is supported by the National Science Foundation under Grant No. DMR-94-03441, in part by the Donors of The Petroleum Research Fund, administered by the American Chemical Society, under Grant PRF # 27240-AC5, and by the University of California at Davis Graduate Research Award.

References

1. G.A. Somorjai: *Chemistry in Two Dimensions: Surfaces* (Cornell Univ. Press, Ithaca, NY 1981)
2. J. Topping: Proc. R. Soc. (London) A **114**, 67 (1927)
3. For example, K. Christmann, O. Schober, G. Ertl, M. Neumann: J. Chem. Phys. **60**, 4528 (1974)
4. J.D.E. McIntyre, D.E. Aspnes: Surf. Sci. **24**, 417 (1971)
D.E. Aspnes: IEEE J. QE **25**, 1056 (1989)
K. Hingerl, D.E. Aspnes, I. Kamiya: Surf. Sci. **287–288**, 686 (1993)
D.E. Aspnes: Surf. Sci. **307–309**, 1017 (1994)
J.F. McGilp: J. Phys. C2, 7985 (1990); Prog. Surf. Sci. **49**, 1 (1995)
M. Kuball, M.K. Kelly, P.V. Santos, M. Cardona: Phys. Rev. B **50**, 8609 (1994)
5. G.A. Bootsma, F. Meyer Surf. Sci. **14**, 52 (1969)
6. X.-D. Xiao, Y. Xie, Y.R. Shen: Surf. Sci. **271**, 295 (1992)
7. X.D. Zhu, A. Lee, A. Wong: Appl. Phys. A, 317 (1991)
8. H.W.K. Tom, C.M. Mate, X.D. Zhu, J.E. Crowell, T.F. Heinz, G.A. Somorjai, Y.R. Shen: Phys. Rev. Lett. **52**, 348 (1984)
9. X.D. Zhu, Y.R. Shen, R. Carr: Surf. Sci. **163**, 114 (1985)
10. S.N. Jasperson, S.E. Schnatterly: Rev. Sci. Instrum. **40**, 761 (1969)
11. K. Christmann, R.J. Behm, G. Ertl, M.A. Van Hove, W.H. Weinburg: J. Chem. Phys. **70**, 4168 (1979)
12. K.H. Frank, R. Dudde, H.J. Sagner, W. Eberhardt: Phys. Rev. B **39**, 940 (1989)
13. F. Greuter, I. Strathy, E.W. Plummer, W. Eberhardt: Phys. Rev. B **33**, 736 (1986)
F.J. Himpsel, J.A. Knapp, D.E. Eastman: Phys. Rev. B **19**, 2872 (1979)
14. W. Reimer, Th. Fink, J. Küppers Surf. Sci. **193**, 259 (1988)
15. C.Y. Fong: private communication
16. I. Langmuir: J. Am. Phys. Soc. **28**, 28 (1928)
17. J. Lapujoulade, K.S. Neil: J. Chem. Phys. **57** 3535 (1972)
J. Lapujoulade, K.S. Neil: Surf. Sci. **35**, 288 (1973)
18. M. Bienfait, J.A. Venables: Surf. Sci. **64**, 425 (1977)
M. Bienfait, J.A. Venables: Surf. Sci. **61**, 667 (1976)
19. J. Suzanne, J.P. Coulomb, M. Bienfait: Surf. Sci. **40**, 414 (1973)
44, 141 (1974); **47**, 204 (1975)
A. Thomy, X. Duval: J. Chem. Phys. **67**, 1101 (1970)
G. Quentel, J.M. Rickard, R. Kern: Surf. Sci. **50**, 343 (1975)
20. A. Glachant, U. Bardi: Surf. Sci. **87**, 187 (1979)
A. Glachant, M. Jaubert, M. Bienfait, G. Boato: Surf. Sci. **115**, 219 (1981)
21. M.A. Chester, M. Hussain, J. Pritchard: Surf. Si. **35**, 161 (1973)
22. C.T. Rettner, D.S. Bethune, E.K. Schweizer: J. Chem. Phys. **92**, 1442 (1990)
23. K. Kern, R. David, P. Zeppenfeld, G. Comsa: Surf. Sci. **195**, 353 (1988)
24. H.R. Siddiqui, P.J. Chen, X. Guo, J.T. Yates, Jr.: J. Chem. Phys. **92**, 7690 (1990)
25. B.E. Nieuwenhuys, D. Th. Meijer, W.M.H. Sachtler: Phys. Stat. Sol. (a) **24**, 115 (1974)
26. J. Ungris, L.W. Bruch, E.R. Moog, M.B. Webb: Surf. Sci. **109**, 522 (1981)
27. P.W. Palmberg: Surf. Sci. **25**, 598 (1971)
28. E.R. Moog, M.B. Webb: Surf. Sci. **148**, 338 (1984)
29. K. Wandelt, J.E. Hulse: J. Chem. Phys. **80**, 1340 (1984)
30. K. Christmann, J.E. Demuth: Surf. Sci. **120**, 291 (1982)
31. M.J. Dresser, T.E. Madey, J.T. Yates: Surf. Sci. **42**, 553 (1974) C.
Wang, R. Gomer: Surf. Sci. **91**, 533 (1980)
32. R. Opila, R. Gomer: Surf. Sci. **112**, 1 (1981)
33. P. Dolle, M. Alnot, J.J. Ehrhardt, A. Thomy, A. Cassuto: Surf. Sci. **152/153**, 620 (1985) D. Fargues, P. Dolle, M. Alnot, J.J. Ehrhardt: Surf. Sci. **214**, 187 (1988)
34. D.L. Meixner, S.M. George: J. Chem. Phys. **98**, 9115 (1993)
35. P.S. Weiss, D.M. Eigler: Phys. Rev. Lett. **69**, 2240 (1992) D.M. Eigler: private communication
36. S. Liu, Z. Zhang, G. Cosma, H. Metiu: Phys. Rev. Lett. **71**, 2967 (1993)